Exploiting Plasmon-Induced Hot Electrons in Molecular Electronic Devices

David Conklin,[†] Sanjini Nanayakkara,[†] Tae-Hong Park,[‡,∥] Marie F. Lagadec,[§] Joshua T. Stecher,[⊥] Xi Chen,[†] Michael J. Therien,[⊥] and Dawn A. Bonnell[†,*]

[†]Department of Materials Science & Engineering and [‡]Department of Chemistry, University of Pennsylvania, Philadelphia, Pennsylvania 19104, United States, [§]Department of Materials, ETH Zurich, Zurich CH-8093, Switzerland, and [⊥]Department of Chemistry, French Family Science Center, Duke University, Durham, North Carolina 27708, United States. [∥]Present address: Nuclear Chemistry Research Division, Korea Atomic Energy Research Institute, Daejeon 305-353, Republic of Korea.

ABSTRACT Plasmonic nanostructures can induce a number of interesting responses in devices. Here we show that hot electrons can be extracted from plasmonic particles and directed into a molecular electronic device, which represents a new mechanism of transfer from light to electronic transport. To isolate this phenomenon from alternative and sometimes simultaneous mechanisms of plasmon–exciton interactions, we designed a family of hybrid nanostructure devices consisting of Au nanoparticles and optoelectronically functional porphyin molecules that enable precise control of electronic and optical properties. Temperature- and wavelength-dependent transport measurements are analyzed in the context of optical absorption spectra of the molecules, the Au particle arrays, and the devices. Enhanced photocurrent associated with exciton generation in the molecule is distinguished from enhancements due to plasmon interactions. Mechanisms of plasmon-induced current are examined, and it is found that hot electron generation can be distinguished from other possibilities.

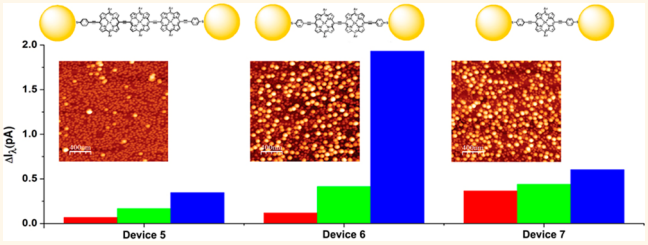

KEYWORDS: plasmon · nanoparticle · molecular electronics · photoconductance · electronic transport · hot electron

An exciting advance in the arena of photovoltaic devices is the incorporation of plasmonic nanostructures. The plasmonic component serves to enhance or direct optical scattering, which can yield interesting properties. Plasmons are collective oscillations of electrons that can be excited with optical radiation or electrons. The plasmon resonance is determined by the composition, size, and shape of the particles and the dielectric properties of the environment. Plasmons produce a large local electrical field resulting in enhanced optical scattering that has been exploited in surface-enhanced Raman spectroscopy[1,2] and nano-antennae-based devices.[3] Plasmonic nanostructures can be designed to enhance scattering; examples include enhanced photoluminescence in quantum dots,[4] increased absorption in solar cells,[5] and increased photoconduction in metal–organic hybrids.[6] Recent attention is focused on energy transfer between nanostructures.[7,8] For example plasmonic enhancement in nanorods facilitates Förster resonant energy transfer in a directional manner.[9] In these cases, optical energy is transferred and excitons are created, illustrating that plasmonic interactions can increase electron/hole generation in a device by scattering light to increase absorption, by directing light to absorbers and exchanging optical energy between adjacent particles.

Optically excited plasmons can dephase to produce electron–hole pairs within a metal. These "hot" carriers relax through electron collisions, coupling to lattice vibrations, emission, or coupling to nanostructures.[10,11] In photoemission[12,13] and during electron energy loss measurements in electron microscopy, hot electrons are emitted under very high electric fields. Hot electrons have been implicated in enhanced photocatalysis,[14–17] and recently, Mukerjee *et al.*[18] have explicitly demonstrated plasmon-induced dissociation of hydrogen. The ability to exploit hot electrons between solids has been demonstrated,[19,20] and Knight *et al.*[21]

* Address correspondence to bonnell@seas.upenn.edu.

Received for review March 3, 2013 and accepted April 3, 2013.

Published online 10.1021/nn401071d

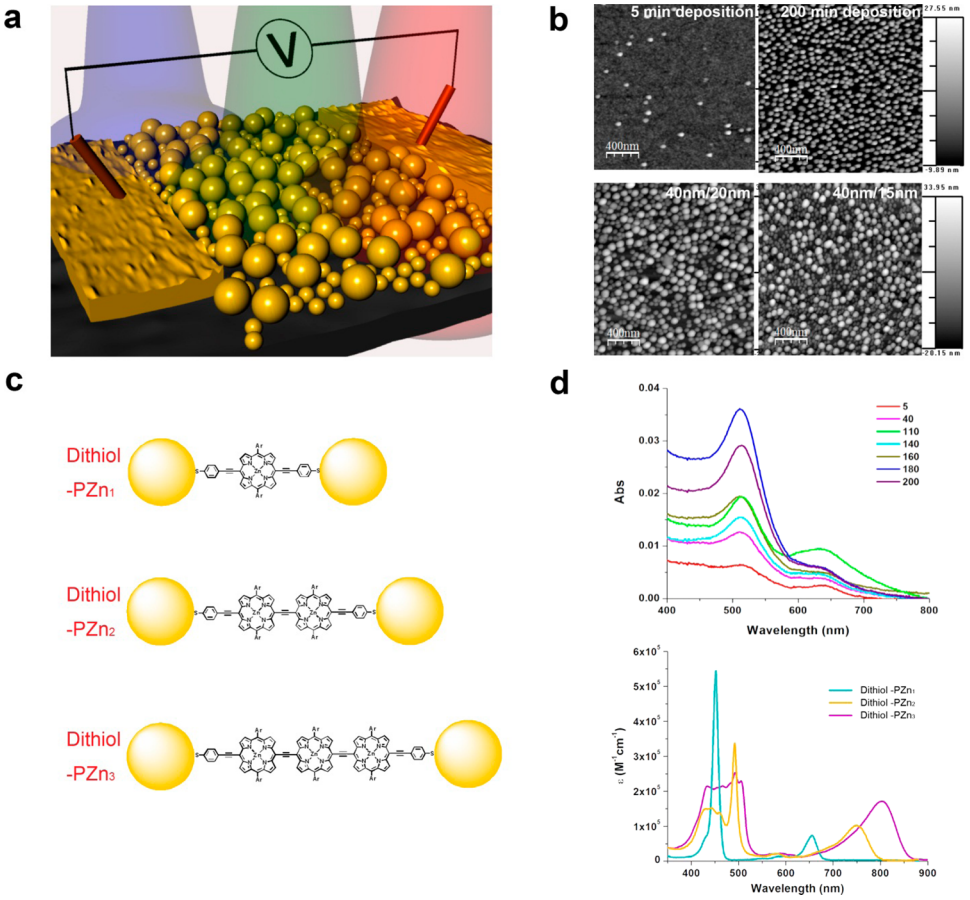

Figure 1. Family of hybrid optoelectronic devices with controlled variation in photoconduction properties. (a) Arrays of Au nanoparticles are deposited on insulating substrates and linked with thiophenylethynyl-terminated porphyrin molecules (c). (b) Atomic force microscopy illustrates the control of size and density of monodispersed and bimodal distributions of nanoparticles. (d) Absorption properties of dithiol-PZn$_n$-linked Au nanoparticles in devices (top) are compared with those of the dithiol-PZn$_n$ supermolecules in THF solution (bottom).

have demonstrated hot electron transfer in a Schottky doide.

A question arises as to whether hot carriers associated with the plasmon resonance can be liberated and harnessed into an optoelectronic device. We have previously demonstrated plasmon-induced current in Au-porphyrin nanostructures by field focusing,[6] the same mechanism that operates in SERS. The ability to exploit plasmon-induced hot electrons in molecular devices would enable a new strategy of device design with the potential of dramatically increased light harvesting. In order to determine if it is possible to extract hot carriers from plasmons that can contribute directly to electrical current in molecular electronics, we design a family of hybrid optoelectronic devices consisting of Au plasmonic nanoparticles linked with photoactive, thiophenylethynyl-terminated metalloporphyrin structures. This platform allows systematic variations in the optical absorption of the molecules and the plasmon resonances. Combinations of these variations yield devices in which the mechanisms of photocurrent enhancement can be systematically investigated.

Figure 1 shows the attributes that are controlled to produce devices with the necessary property variations. Gold nanoparticle arrays are connected to contact pads that enable temperature- and wavelength-dependent measurement of electronic transport. The particle size, distribution, and density are varied to adjust the plasmon resonance energy of the arrays (Supporting Information). The top two images in Figure 1b illustrate the increased coverage with deposition time. The bottom two show the morphology difference of a bimodal array with 40 nm/20 nm particles and one with 40 nm/15 nm particles. Figure 1b illustrates typical array morphologies; the range of optical properties is shown in the electronic absorption spectra of Figure 1d. As expected, the primary Au plasmon resonance is evident at ~524 nm; the peak position is dominated by the 40 nm particles and does not shift much, while the peak amplitude increases with particle coverage. Coverage increases with deposition time from 5 to 200 min. The peak at ~640 nm is broad; the spectral breadth of this peak varies with particle size, distribution, spacing, and aggregation, while its maximum reflects the average degree of

particle−particle electronic coupling.[22] See Supporting Information for analysis protocol.

The separation of the particles is such that the devices do not conduct current until the molecular linkers are attached. Optically active α,ω-dithiol-terminated *meso*-to-*meso* ethyne-bridged (porphinato)-zinc(II) supermolecules (dithiol-PZn$_n$) shown in Figure 1c were synthesized as previously reported.[23−26] These molecules exhibit near barrier-less charge transport and global electronic delocalization. The optical absorption spectra (Figure 1d) show that dithiol-PZn$_1$ manifests a high oscillator strength sharp absorption band ($S_0 \rightarrow S_2$) at ∼450 nm and a quasi-allowed absorption ($S_0 \rightarrow S_1$) centered at ∼650 nm that is polarized along the highly conjugated molecular axis. In contrast, dithiol-PZn$_2$ and dithiol-PZn$_3$ feature broad $S_0 \rightarrow S_2$ absorption manifolds that span a ∼375−525 nm spectral domain and identically polarized long wavelength $S_0 \rightarrow S_1$ absorptions that gain in intensity and progressively red shift with increasing numbers of PZn units (Figure 1d). Note that $S_2 \rightarrow S_1$ electronic relaxation occurs at unit quantum yield in the femtosecond time domain; excitation into either absorptive manifold thus gives rise to ultrafast formation of identical low energy electronically delocalized S_1 states.

To examine the mechanisms of photoconduction, the temperature and wavelength dependences of the transport properties were measured, and we consider first the case of the devices functionalized with dithiol-PZn$_1$. As shown previously,[27] the dark transport mechanism of porphyrin-linked AuNP devices can be described as thermally assisted tunneling, which consists of both thermionic emission and tunneling and is represented by eq 1, where I is the current, V is the applied voltage, T is the temperature, k is the Boltzmann constant, $t(y)$ is an elliptical function, and Θ is a function of both elliptic functions $v(y)$ and $t(y)$.

$$I = \frac{V}{2\pi}\left(\frac{kTt(y)}{2\pi}\right)^{1/2} \exp\left(-\frac{\phi}{kT} + \frac{V^2\Theta}{24(kT)^3}\right) \quad (1)$$

$$\frac{d\ln I}{dV} = V^{-1} + \left(\frac{V\Theta}{12(kT)^3}\right) \quad (2)$$

Differential analysis based on eq 2 was carried out on over 20 devices. The fits (red dotted lines) to the transport data shown in the Supporting Information (Figure S3) illustrate agreement between this model and the experiment. The fit factor Θ is a function of applied field and the barrier height. The fits of eq 2, shown yield $\Theta = 1.34 \times 10^{-8}$ to 3.69×10^{-7}, for the range of arrays tested. These values correspond to the situation where the number of active junctions in the array is small and barrier heights are on the order of 10−30 meV.

Further, the global conductivity of the devices is related to the barrier height so that comparing devices

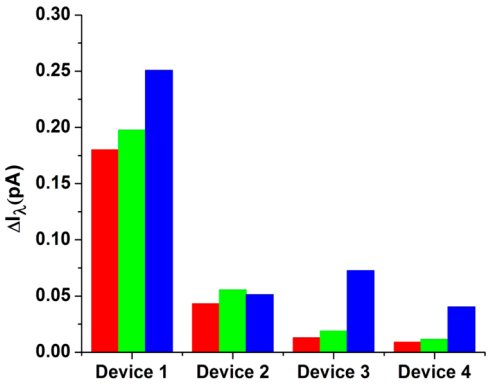

Figure 2. Photocurrent at 180 K, conductance while illuminated with 405 (shown in blue), 533 (shown n green), and 655 nm (shown in red) light, subtracted from dark conductance, of four hybrid devices that utilize dithiol-PZn$_1$ linkers.

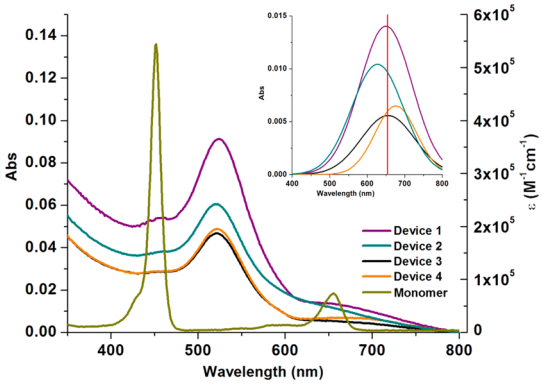

Figure 3. Optical absorption spectra of the four dithiol-PZn$_1$-linked AuNP arrays (left axis is absorption in arbitrary units) relative to the dithiol-PZn$_1$ (monomer) solution spectrum (right axis). Inset displays a closer examination of the high wavelength peak located at ∼650 nm.

of similar conductivity implies that the barrier height is nearly constant. Figure 2 shows the photoconductance of four devices containing dithiol-PZn$_1$ linkers that display differences in nanoparticle coverage and plasmon coupling. The photocurrent in Figure 2 is the effect of optical illumination on electronic transport. The magnitude of the photocurrent scales with the height of the plasmon resonance peak and with nanoparticle coverage, as shown in Figure 1d. Therefore, we compare here device 1, which has higher coverage, with devices 2−4. These devices consist of similar 40 nm/20 nm particle distributions with the exception that device 1 has a higher coverage. The enhancement due to blue (405 nm) excitation is the largest; green-induced (533 nm) and red-induced (655 nm) enhancements are similar to each other in magnitude. Figure 3 superimposes the absorption spectra from the four arrays with that of the monomer. Note that, for the dithiol-PZn$_1$-based devices, green light overlaps the plasmon primary peak but no molecular absorption band, red overlaps the second plasmon peak and the low energy molecular absorption, and blue does not

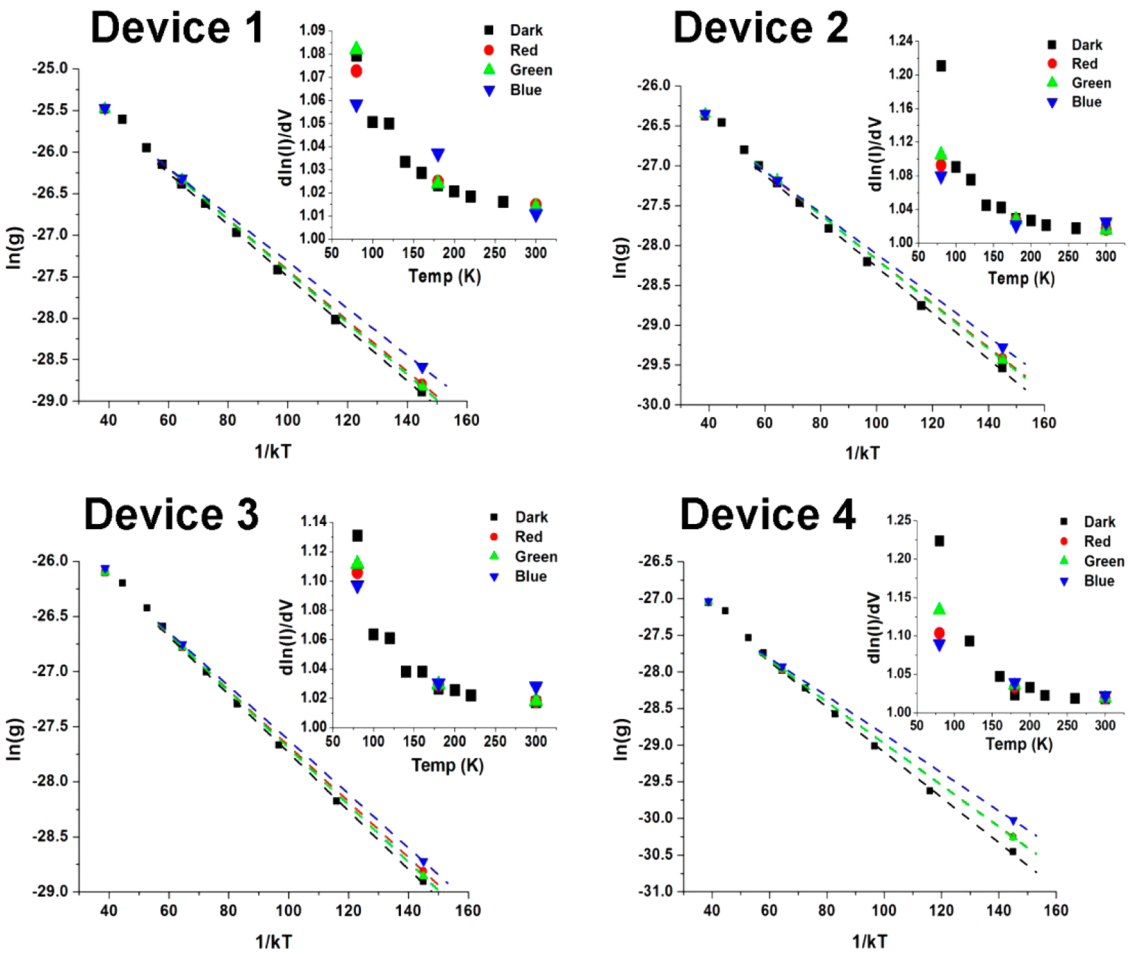

Figure 4. Temperature dependence of conductance (Arrhenius analysis) and dln(*I*)/d*V* (differential analysis) in inset for the four devices in Figure 2.

overlap any plasmon peak but overlaps the shoulder of the $S_0 \rightarrow S_2$ molecular absorption.

Photocurrent enhancement could result from several possible mechanisms. (a) Plasmon-induced electrical fields can focus photon flux to the junction and increase optical absorption, that is, the nanoantenna effect. (b) The plasmon could reduce the tunneling activation barrier and therefore increase the tunneling transmission probability. (c) Absorption in the metal could cause a temperature increase. (d) Photoassisted tunneling could occur. (e) Plasmon-generated charge carriers, "hot electrons", could contribute directly to the current. We consider each possibility in the context of the dithiol-PZn_1-based devices.

For the case of the dithiol-PZn_1-based devices, photocurrent is observed at all wavelengths. With exposure to blue light, no plasmons are excited since the wavelength is far from the plasmon resonance (Figure 3). The observed photocurrent derives from exciton creation in the porphyrinic linker, which can be referred to as conventional photoconduction. Red illumination excites both the plasmon peak and the molecular absorption: exciton generation occurs, and field focusing increases the local photon flux, further contributing to photocurrent. Green illumination, in contrast, excites only Au plasmons; note that, at 533 nm, dithiol-PZn_1 features minimal absorptive oscillator strength. Consequently, while the field focusing, nanoantenna effect certainly operates at this wavelength, it does not lead to increased charge carrier concentration within the molecule. There must be other mechanisms by which the plasmons enhance the photocurrent at an irradiation wavelength of 533 nm.

To determine whether the tunneling activation energy is affected by the plasmon excitation, two analyses of the temperature dependence of transport were performed (Figure 4). In the classical Arrhenius analysis, the slope of the ln(conductance) *versus* 1/*T* yields an "apparent" activation energy. The comparisons from 180 to 300 K find negligible differences in the activation energy of photocurrent compared to dark current for all irradiation wavelengths. More rigorously, fitting the temperature dependence of light-induced conductance to the thermally assisted tunneling model and again comparing the dark current and photocurrent reveals that there is no difference in activation energy (inset in Figure 4). Therefore, plasmon excitation is not affecting the tunneling barrier.

Govorov *et al.*[28] calculated the temperature increase of gold nanoparticles in liquid. Using this equation to estimate the order of temperature increase ΔT for gold nanoparticles in air, all terms in the heat transfer equation are the same except for the thermal conductivity, k, and dielectric constant, ε, of air compared to water, $\Delta T \propto 1/k$ and $\Delta T \propto \varepsilon/(\varepsilon + \varepsilon_m)$. The thermal conductivity of air is 0.024 W/min K and for water is 0.6 W/min K, which leads to an estimate of a higher temperature increase by a factor of 30. The dielectric constant of air is 1 compared to 1.8 for water leading to a decrease of about a factor of 2. The light flux in our measurements ranges from 0.83 to 3.08 W/cm^2, which leads to negligible temperature increase even assuming maximum absorption for particles up to hundreds of nanometers in diameter.

In an analogous calculation for heat dissipation through a SiO_2 substrate, Mangold *et al.*[29] estimate a temperature increase of 0.55 K for a gold nanoparticle array on a 150 nm substrate using $Q = \lambda \Delta T/d$, where Q is heat conduction, λ is the thermal conductivity of silica, and d is the substrate thickness. This calculation is for a light flux of 1 kW/cm^2. In our configuration, the substrate thickness is a factor of 1000 larger and the flux is a factor of 1000 smaller, leading to an estimate of negligible temperature rise.

Photoassisted tunneling is a mechanism analogous to microwave rectification,[30,31] whereby the plasmon induces an oscillating voltage between particles that allows electron tunneling between the particles at the plasmon frequency. The superposition of a small dc voltage biases the tunneling probability resulting in additional dc current. Two types of control samples were constructed to test for this process: arrays with no molecules and arrays linked with a conducting but not optically active dithiol-terminated molecule (4,4′-(1,4-phenylenebis(ethyne-2,1-diyl))dibenzenethiol). In all cases, there was no photocurrent at any illumination wavelength, indicating that photoassisted tunneling between the metal particles does not occur (Supporting Information Figure S4 and Figure S5).

The remaining possibility is that "hot" charge carriers induced by the plasmon contribute to the photocurrent. The results in Figures 2 and 3 clearly distinguish situations in which molecular absorption, plasmon-mediated absorption, and plasmon-induced tunneling contribute to the photocurrent. With blue (405 nm) illumination, exciton generation in the molecule occurs but there is no plasmonic excitation. With red light (655 nm), exciton generation and plasmonic focusing can occur. Little exciton generation in the molecule can occur with 533 nm excitation given its low extinction absorption at this wavelength, so neither conventional photoexcitation nor the nanoantennae effect operates effectively at this wavelength. Yet photocurrent is observed at this wavelength in all devices that utilize PZn_1 linkers. In plasmon-induced transport, an additional source of carriers is available for tunneling, either in resonant tunneling through the molecule or *via* an inelastic process, depending on the energy. The photocurrent measured at 533 nm indicates that it is possible to extract these carriers in an electronic device, in this case based on molecular junctions. This source of current is, in principle, large and could lead to extremely high energy transduction efficiencies.

The femtosecond lifetimes of the plasmonic state imply that the extraction of electron/holes is unlikely; however, several photochemical and photoemission studies provide evidence that slower relaxation channels can exist. Surface photochemistry on rough Ag electrodes and on metal nanocrystals has been induced by optical excitation.[32−35] These reactions require electron or hole exchange (*i.e.*, vibration of the carriers). Gerber and colleagues[13] observed enhanced electron emission in a photoemission measurement that interrogated Ag particles at the plasmon resonance. Nakanishi *et al.*[36] designed an array-based chemical sensor that implied that plasmons may involve hot electrons, and recently, Knight *et al.*[21] suggested that hot electrons can overcome a Schottky barrier. Meanwhile, theoretical calculations by Zelinskyy and May[37] provide evidence that plasmon−molecule interactions might induce increased measurable current at metal junctions, in spite of the expected short plasmon lifetime. Our results unambiguously show that, by imposing an electric field between the nanoparticles, hot electrons can be extracted and can contribute to the properties of a molecular electronic and/or energy harvesting device.

The analyses of the devices based on the PZn_1 linker distinguish plasmon-induced hot carrier transport from exciton formation as the molecular absorption manifolds lie outside the wavelength range that gives rise to plasmon excitation. While this demonstrates that plasmon-induced hot carriers can contribute to device function, it also implies that more complex behavior can be engineered with different constituent choices. Figures 5 and 6 compare the behavior of devices fabricated with dithiol-PZn_2 and dithiol-PZn_3 linkers to those that feature dithiol-PZn_1 connectivity between nanoparticles. The nanoparticle arrays in devices 6 and 7 are similar as is evident in the AFM images of the morphology (Figure 5a). Both consist of bimodal arrays with approximately equal coverage of 40 and 15 nm particles; consequently, they exhibit similar plasmonic properties as indicated in the absorption spectra (Figure 6b). The primary difference between these two devices lies in the optical properties of the porphyrin-based linker. In device 7, the exciton-based photocurrent results from 405 nm illumination; the plasmon-induced hot electron current results from 533 nm illumination, and a similar magnitude of photocurrent at 655 nm can be attributed to a combination of field focusing and hot electrons. The broad absorption band with high oscillator strength for the dithiol-PZn_2 $S_0 \rightarrow S_2$ transitions in device 6 results in

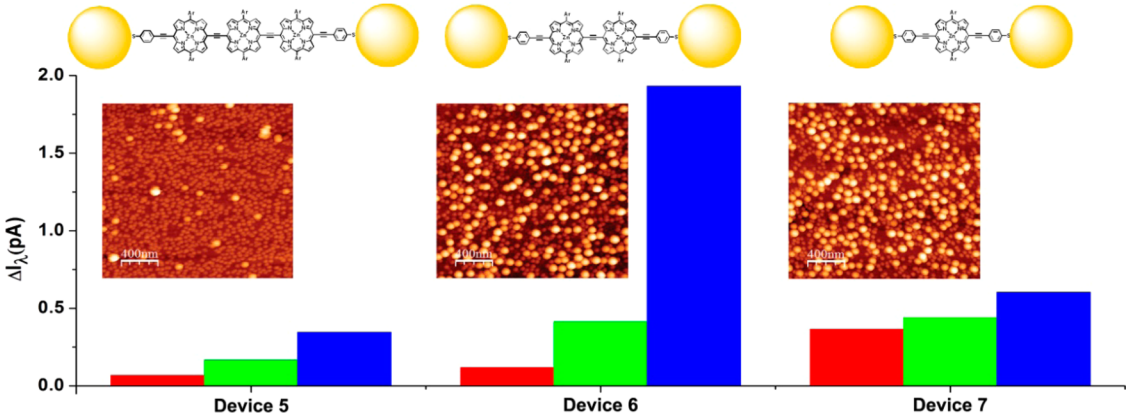

Figure 5. Photoconduction at 180 K of hybrid devices linked with dithol-PZn$_3$, dithol-PZn$_2$, and dithol-PZn$_1$. Conductance while illuminated with 405 (shown in blue), 533 (shown n green), and 655 nm (shown in red) light, subtracted from dark conductance is compared.

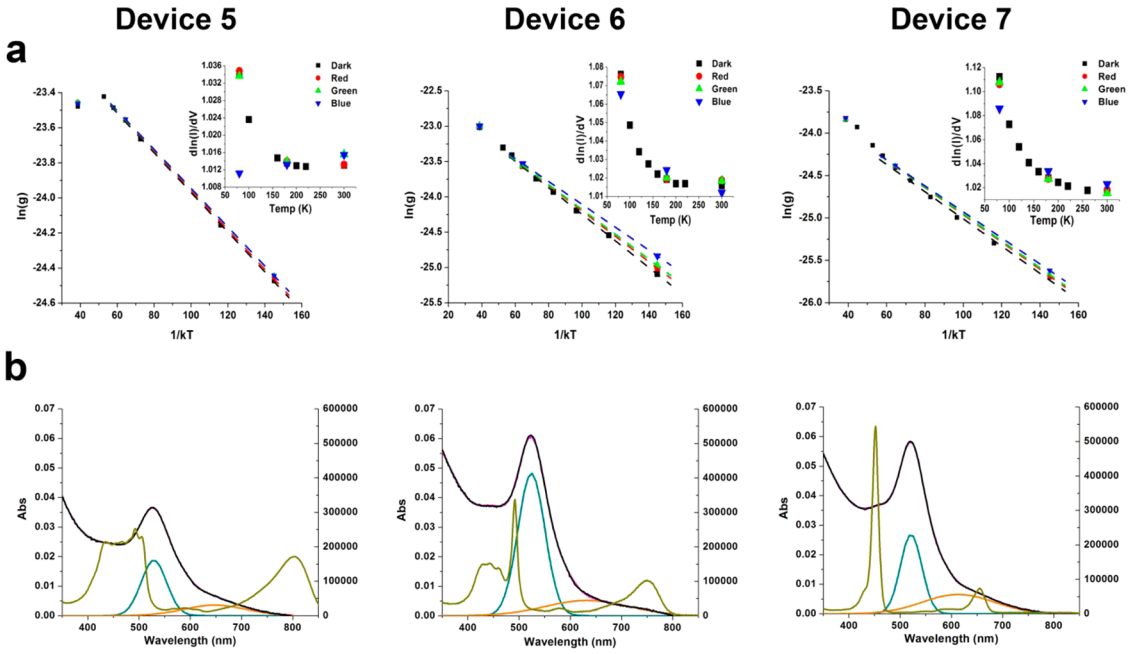

Figure 6. (a) Temperature dependence of conductance (Arrhenius analysis). Inset: dln(*I*)/d*V* (differential analysis). (b) Optical absorption spectra of the dithiol-PZn$_n$-linked Au nanoparticles in devices (black, left axes) overlaid with the molecular absorption spectra (tan, right axes) and the first (aqua) and second (orange) plasmon peaks.

a larger absorption cross section at 405 nm relative to that manifest in device 7, which relies on a dithiol-PZn$_1$ linker.

Whereas the 405 nm illumination wavelength excites the molecular linker on the high energy shoulder ($\varepsilon \sim 0.1 \times 10^5$ M^{-1} cm^{-1}) of the $S_0 \rightarrow S_2$ manifold in device 7, the corresponding extinction coefficient for the dithiol-PZn$_2$ linker of device 6 at 405 nm is approximately 1 order of magnitude higher. This greater extinction coefficient for blue excitation in device 6 gives rise to a higher photocurrent contribution that derives from exciton generation. Similarly, the long wavelength $S_0 \rightarrow S_1$ absorption at ~650 nm of the device 7 dithiol-PZn$_1$ linker possesses an exctinction coefficient at 655 nm that exceeds that of the device 6 linker; consequently, for red excitation, a lower degree of photocurrent enhancement is observed for device 6 relative to that measured for device 7. Device 5 features a dithiol-PZn$_3$ linker and Au nanoparticles that are predominately 15 nm in diameter, which contrasts that for devices 6 and 7 which feature approximately equal coverage of 40 and 15 nm particles and accounts for the observed differences in the intensity of the plasmon peaks for these devices. This combination of linker- and AuNP-dependent absorptive properties results in disparate degrees of photocurrent enhancement for blue, green, and red light excitation relative to that observed for devices 6 and 7. The lower red photocurrent in devices 5 and 6 relative that measured for device 7 suggests that, for long wavelength excitation, maximal photocurrents should be observed when the laser irradiation wavelength approaches the $S_0 \rightarrow S_1$ absorption maximum, which is polarized along the

highly conjugated molecular axis; note that for the dithiol-PZn_3 and dithiol-PZn_2 linkers of devices 5 and 6, this wavelength corresponds, respectively, to ~750 and 800 nm. These differences serve to illustrate how the design of both the molecular absorption and the plasmon resonances of the arrays could be used to engineer a wide range of device properties.

In summary, we demonstrate that hot electrons can be extracted from plasmons and exploited in molecular electronic optoelectronic devices. This mechanism has the potential to revolutionize energy harvesting and optoelectronic circuit design since hot electron generation is more efficient than exciton generation. The ability to tune optical interactions and transport mechanisms by controlling particle material, size, and separation along with molecular optical and electronic structures suggests a new strategy for photovoltaic device platforms.

METHODS

Device Fabrication. The devices were fabricated by immersion of glass substrates functionalized with 3-(aminopropyl)-trimethoxysilane (APTMS) in solutions of citrate-stabilized gold nanoparticles (Ted Pella). The nanoparticle size distribution and surface density were controlled by the immersion time in the solution (Figure S1). Gold contact pads with a separation of approximately 70 μm were deposited by a thermal evaporation through a physical mask. Transport properties of the arrays were measured. Molecular linkers were attached to those arrays that exhibited no conductivity. Attachment of the optically active α,ω-dithiol-terminated *meso*-to-*meso* ethyne-bridged (porphinato)zinc(II) supermolecules (dithiol-PZn_n) was achieved under inert atmosphere using solvents distilled and subjected to freeze−pump−thaw cycles in liquid nitrogen to remove water and residual gases. Approximately 1 μM concentration solutions of each *S*-acetyl-protected dithiol-PZn_n derivative were prepared in distilled tetrahydrofuran and 4 μL/mL of NH_4OH, exposing the thiol functionality. Devices were prepared by incubating AuNP arrays with such solutions for ~1 h.

Measurement Protocols. Conductivity measurements were conducted with an electrometer (Keithley 6517A) before attachment of the dithiol-PZn_n complexes to ensure that there was no conductance prior to attachment of the molecular linkers. Temperature-dependent conductance measurements of AuNP arrays linked with monomer (PZn_1), dimer (PZn_2), and trimer (PZn_3) supermolecules were carried out from room temperature to 80 K. Wavelength-dependent conductance measurements performed under illumination with red (655 nm), green (533 nm), and blue (405 nm) laser diodes. The power densities for the red, green, and blue laser diodes were 0.83, 1.81, and 3.08 mW/mm^2, respectively. Reported photoconductance values are normalized by photon flux.

Design and Synthesis. The synthetic route to *S*-acetyl-protected dithiol-PZn_n compounds is illustrated in Figure S2. Synthetic procedures and characterization data for these compositions have been reported elsewhere.[6,26]

Optical Absorption Fitting Procedures. The optical properties of the AuNP arrays were determined by optical absorption spectroscopy. The optical spectra were analyzed using standard fitting software (Origin). The spectra were fit with Gaussian peaks located at approximately 200, 525, and 650 nm to mimic the substrate, primary, and coupled plasmon resonances, respectively, and two at the known absorption maximum for the AuNP-porphyrin complexes. Peak positions and heights were varied until regression analysis yielded the optimized fit. In all cases, the R^2 factor was $\geq$0.999.

Conflict of Interest: The authors declare no competing financial interest.

Acknowledgment. M.J.T. is grateful to the Division of Chemical Sciences, Geosciences, and Biosciences, Office of Basic Energy Sciences of the U.S. Department of Energy through Grant DE-SC0001517, for funding the development of these electro-optically functional porphyrin-based supermolecules, Nano/Bio Interface Center NSF Grant NSEC DMR08-32802 is acknowledged for support of the research on the nanoparticle arrays as well as use of facilities.

Supporting Information Available: Gold nanoparticle arrays morphology, synthesis of *S*-acetyl-protected dithiol-PZn_n structures, differential analysis of the dark current transport mechanism, transport properties of nanoparticle arrays without linkers and with oligo(phenylene ethynylene) (OPE) linkers. This material is available free of charge *via* the Internet at http://pubs.acs.org.

REFERENCES AND NOTES

1. Willets, K. A.; Van Duyne, R. P. Localized Surface Plasmon Resononance Spectroscopy and Sensing. *Annu. Rev. Phys. Chem.* **2007**, *58*, 267–297.
2. Johnson, R. C.; Li, J.; Hupp, J. T.; Schatz, G. C. Hyper-Rayleigh Scattering Studies of Silver, Copper, and Platinum Nanoparticle Suspensions. *Chem. Phys. Lett.* **2002**, *356*, 534–540.
3. Mueschlegel, P.; Eisler, H.-J.; Martin, O. J. F.; Hecht, B.; Pohl, D. W. Resonant Optical Antennas. *Science* **2005**, *308*, 1607–1609.
4. Munechika, K.; Chen, Y.; Tillack, A. F.; Kulkarni, A. P.; Plante, I. J.-L.; Munro, A. M.; Ginger, D. S. Spectral Control of Plasmonic Emission Enhancement from Quantum Dots near Single Silver Nanoprisms. *Nano Lett.* **2010**, *10*, 2598–2603.
5. Nakayama, K.; Tanabe, K.; Atwater, H. A. Plasmonic Nanoparticle Enhanced Light Absorption in GaAs Solar Cells. *Appl. Phys. Lett.* **2008**, *93*, 121904(1)–121904(3).
6. Banerjee, P.; Conklin, D.; Nanayakkara, S.; Park, T. H.; Therien, M. J.; Bonnell, D. A. Plasmon-Induced Electrical Conduction in Molecular Devices. *ACS Nano* **2010**, *4*, 1019–1025.
7. Zhdanova, V. P.; Hägglunda, C.; Kasemo, B. Relaxation of Plasmons in nm-Sized Metal Particles Located on or Embedded in an Amorphous Semiconductor. *Surf. Sci.* **2005**, *599*, L372–L375.
8. Kagan, C. R.; Murray, C. B.; Bawendi, M. G. Long-Range Resonance Transfer of Electronic Excitations in Close-Packed CdSe Quantum Dot Solids. *Phys. Rev. B* **1996**, *54*, 8633–8643.
9. Lee, J.; Govorov, A. O.; Kotov, N. A. Bioconjugated Superstructures of CdTe Nanowires and Nanoparticles: Multistep Cascade Forster Resonance Energy Transfer and Energy Channeling. *Nano Lett.* **2005**, *5*, 2063–2069.
10. Liau, Y.; Unterreiner, A. N.; Chang, Q.; Scherer, N. F. Ultrafast Dephasing of Single Nanoparticles Studied by Two-Pulse Second-Order Interferometry. *J. Phys. Chem. B* **2001**, *105*, 2135–2142.
11. Hu, M.; Hartland, G. V. Heat Dissipation for Au Particles in Aqueous Solution: Relaxation Time *versus* Size. *J. Phys. Chem. B* **2002**, *106*, 7029–7033.
12. Nollé, É. L.; Shchelev, M. YA. Photoelectron Emission Caused by Surface Plasmons in Silver Nanoparticles. *Tech. Phys. Lett.* **2004**, *30*, 304–306.
13. Merschdorf, M.; Pfeiffer, W.; Thon, A.; Voll, S.; Gerber, G. Photoemission from Multiply Excited Surface Plasmons in Ag Nanoparticles. *Appl. Phys. A: Mater. Sci. Process.* **2000**, *71*, 547–552.

14. Wu, X.; Thrall, E. S.; Liu, H.; Steigerwald, M.; Brus, L. Plasmon Induced Photovoltage and Charge Separation in Citrate-Stabilized Gold Nanoparticles. *J. Phys. Chem. C* **2010**, *114*, 12896–12899.
15. Christopher, P.; Xin, H.; Linic, S. Visible-Light-Enhanced Catalytic Oxidation Reactions on Plasmonic Silver Nanostructures. *Nat. Chem.* **2011**, *3*, 467–472.
16. Lee, J.; Mubeen, S.; Ji, X.; Stucky, G.; Moskovits, M. Plasmonic Photoanodes for Solar Water Splitting with Visible Light. *Nano Lett.* **2012**, *12*, 5014–5019.
17. Wolf, M.; Zhu, X.-y.; White, J. M.; Koschmieder, T. H.; Thompson, J. C. Surface Plasmon Enhanced Photochemistry: $Mo(CO)_6$-Al-Quartz. *J. Chem. Phys.* **1992**, *97*, 7015–7016.
18. Mukherjee, S.; Libisch, F.; Large, N.; Neumann, O.; Brown, L. V.; Cheng, J.; Lassiter, J. B.; Carter, E. A.; Nordlander, P.; Halas, N. J. Hot Electrons Do the Impossible: Plasmon-Induced Dissociation of H_2 on Au. *Nano Lett.* **2013**, *13*, 240–247.
19. Nishijima, Y.; Ueno, K.; Yokota, Y.; Murakoshi, K.; Misawa, H. Plasmon-Assisted Photocurrent Generation from Visible to Near-Infrared Wavelength Using a Au-Nanorods/TiO_2 Electrode. *Phys. Chem. Lett.* **2010**, *1*, 2031–2036.
20. Wang, F.; Melosh, N. Plasmonic Energy Collection through Hot Carrier Extraction. *Nano Lett.* **2011**, *11*, 5426–5430.
21. Knight, M. W.; Sobhani, H.; Nordlander, P.; Halas, N. J. Photodetection with Active Optical Antennas. *Science* **2011**, *332*, 702–704.
22. Kelly, K. L.; Coronado, E.; Zhao, L. L.; Schatz, G. C. The Optical Properties of Metal Nanoparticles: The Influence of Size, Shape and Dielectric Environment. *J. Phys. Chem. B* **2003**, *107*, 668–677.
23. Lin, V. S.-Y.; DiMagno, S. G.; Therien, M. J. Highly Conjugated, Acetylenyl Bridged Porphyrins—New Models for Light-Harvesting Antenna Systems. *Science* **1994**, *264*, 1105–1111.
24. Duncan, T. V.; Susumu, K.; Sinks, L. E.; Therien, M. J. Exceptional Near-Infrared Fluorescence Quantum Yields and Excited-State Absorptivity of Highly Conjugated Porphyrin Arrays. *J. Am. Chem. Soc.* **2006**, *128*, 9000–9001.
25. Susumu, K.; Frail, P. R.; Angiolillo, P. J.; Therien, M. J. Conjugated Chromophore Arrays with Unusually Large Hole Polaron Delocalization Lengths. *J. Am. Chem. Soc.* **2006**, *128*, 8380–8381.
26. Li, Z.; Park, T.-H.; Rawson, J.; Therien, M. J.; Borguet, E. Quasi-Ohmic Single Molecule Charge Transport through Highly Conjugated *meso*-to-*meso* Ethyne-Bridged Porphyrin Wires. *Nano Lett.* **2012**, *12*, 2722–2727.
27. Conklin, D.; Nanayakkara, S.; Park, T. H.; Lagadec, M. F.; Stecher, J. T.; Therien, M. J.; Bonnell, D. A. Electronic Transport in Porphyrin Supermolecule−Gold Nanoparticle Assemblies. *Nano Lett.* **2012**, *12*, 2414–2419.
28. Govorov, A. O.; Zhang, W.; Skeini, T.; Richardson, H.; Lee, J.; Kotov, N. A. Gold Nanoparticle Ensembles as Heaters and Actuators: Melting and Collective Plasmon Resonances. *Nanoscale Res. Lett.* **2006**, *1*, 84–90.
29. Mangold, M. A.; Weiss, C.; Calame, M.; Holleitner, A. W. Surface Plasmon Enhanced Photoconductance of Gold Nanoparticle Arrays with Incorporated Alkane Linkers. *Appl. Phys. Lett.* **2009**, *94*, 161104(1)–161104(3).
30. Ward, D. R.; Hüser, F.; Pauly, F.; Cuevas, J. C.; Natelson, D. Optical Rectification and Field Enhancement in a Plasmonic Nanogap. *Nat. Nanotechnol.* **2010**, *5*, 732–736.
31. Guhr, D. C.; Rettinger, D.; Boneberg, J.; Erbe, A.; Leiderer, P.; Scheer, E. Influence of Laser Light on Electronic Transport through Atomic-Size Contacts. *Phys. Rev. Lett.* **2007**, 086801(1)–086801(4).
32. Maillard, M.; Huang, P.; Brus, L. Silver Nanodisk Growth by Surface Plasmon Enhanced Photoreduction of Adsorbed $[Ag^+]$. *Nano Lett.* **2003**, *3*, 1611–1615.
33. Jin, R.; Cao, Y. C.; Hao, E.; Métraux, G. S.; Schatz, G. C.; Mirkin, C. A. Controlling Anisotropic Nanoparticle Growth through Plasmon Excitation. *Nature* **2003**, *425*, 487–490.
34. Bastys, V.; Pastoriza-Santos, I.; Rodríguez-González, B.; Vaisnoras, R.; Liz-Marzán, L. M. Formation of Silver Nanoprisms with Surface Plasmons at Communication Wavelengths. *Adv. Funct. Mater.* **2006**, *16*, 766–773.
35. Redmond, P. L.; Brus, L. E. "Hot Electron" Photo-Charging and Electrochemical Discharge Kinetics of Silver Nanocrystals. *J. Phys. Chem. C* **2007**, *111*, 14849–14854.
36. Nakanishi, H.; Bishop, K. J. M.; Kowalczyk, B.; Nitzan, A.; Weiss, E. A.; Tretiakov, K. V.; Apodaca, M. M.; Klajn, R.; Stoddart, J. F.; Grzybowski, B. A. Photoconductance and Inverse Photoconductance in Films of Functionalized Metal Nanoparticles. *Nature* **2009**, *460*, 371–375.
37. Zelinskyy, Y.; May, V. Photoinduced Switching of the Current through a Single Molecule: Effects of Surface Plasmon Excitations of the Leads. *Nano Lett.* **2012**, *12*, 446–452.